Computational Materials Science 115 (2016) 170–176

Contents lists available at ScienceDirect

Computational Materials Science

journal homepage: www.elsevier.com/locate/commatsci

Effects of alloying on the behavior of B and S at Σ5 (210) grain boundary in γ-Fe

Yuping Li [a,b,*], Cheng Han [a,b], Caili Zhang [a,b,*], Kun Jia [a], Peide Han [a,b], Xiaolei Wu [c]

[a] College of Materials Science and Engineering, Taiyuan University of Technology, Taiyuan 030024, China
[b] Key Laboratory of Interface Science and Engineering in Advanced Materials of Taiyuan University of Technology, Ministry of Education, Taiyuan 030024, China
[c] State Key Laboratory of Nonlinear Mechanics, Institute of Mechanics, Chinese Academy of Sciences, Beijing 100080, China

ARTICLE INFO

Article history:
Received 17 August 2015
Received in revised form 16 November 2015
Accepted 27 November 2015
Available online 2 February 2016

Keywords:
Alloying
Impurities segregation
γ-Fe
Grain boundary cohesion
DFT

ABSTRACT

To get the atomic scale understanding of impurities induced intergranular embrittlement or enhancement and the control of these effects on austenitic stainless steels, behavior of impurities B and S at γ-Fe grain boundary (GB) and effects of alloying elements (Cr, Ni, Mn, Co, Mo) additions on the cohesive properties of the γ-Fe GB doped by impurities are investigated by performing density functional theory (DFT) calculations. The results showed that, as the GB enhancer and embrittler respectively, impurities B and S tend to stay at the interstitial sites of γ-Fe GB, while alloying elements also can segregate at the GB studied. The presence of all the alloying elements considered can inhibit B GB segregation to some extent due to the higher segregation energies and can impair the enhancement effect of B on GB cohesion. However, these elements almost have no impact on GB segregation and embrittlement effect of S, except for Ni, Mn and Mo:Ni and Mo inhibit and improve S GB segregation, respectively; Mn and Mo strongly enhance and reduce S-induced GB embrittlement, respectively. Moreover, the remedial effect of (Cr + Ni), (Cr + Mn) on S-induced GB embrittlement is also discussed. Additional atomic structure and total valence charge density analysis demonstrated and explained our conclusions.

1. Introduction

It is well known that metallic materials' structure and physical properties, especially the mechanical strength, undergo drastic changes by even a small amount of impurity (solute) elements introduction. Grain boundary (GB) segregation of these impurities atoms, which have been studied and demonstrated by abundant researches [1–5], is a very important phenomenon that is responsible for these changes to a large extent. Segregation of sulfur (S) to GBs of metals, for example, can make GB decohesion and thus induces metals brittlement [6–8]. Embrittling and strengthening effects of B, C and P on bcc Fe GB have been studied by Wu et al. [9] using a first-principles calculation. Furthermore, effects of impurities atoms on the other systems, such as Mn on binary Fe–12Mn alloys GB, P, B on Fe alloys, Ni3Al and Ni GB [2,10–14] also have been studied. GB segregation of these impurities elements will considerably modify, generally undesired, the cohesive properties of the GB, resulting in further variations of materials' strength and vulnerability to stress corrosion cracking [11]. Fortunately, GB segregation behavior of impurities is often accompanying with alloying elements existence at or near GB, which can affect, or even remedy the undesired GB cohesion change induced by these impurities. Lee et al. found, for example, that Cr and Mn additions can facilitate the GB embrittlement induced by P segregation, while W and Mo can improve the fracture strength of GB segregated with P [15]. All these suggest that, by cautious alloying, we can repair, and even remove, the undesired impacts or facilitate the beneficial effects of impurity elements on GB.

Thus, with the purpose of predicting and controlling the influence of the GB segregation, understanding the original mechanism of impurities-induced embrittlement and the effect of alloying on GB cohesion is of great importance and has been investigated in amount of researches. Through competition between dislocation crack blunting and brittle separation governing the propagation resistance of an intergranular crack, Rice and Wang established a thermodynamic theory that gives the mechanism of GB embrittlement induced by impurities [16]. Effect of Cr on magnetic and cohesive properties of bcc Fe GB is studied by Wachowicz and Kiejna [10]. Fe and its alloys i.e. austenitic stainless steels (AASs) which are an alloy mainly composed of Fe, Cr, and Ni, are one of the most popular materials and widely used for applications in biomedical, marine, chemical, power, and oil sectors because of

* Corresponding authors at: Taiyuan University of Technology, No. 79 West Yingze Street, Taiyuan 030024, China. Tel.: +86 13994215219, +86 18636860353.
E-mail addresses: yupingli123@163.com (Y. Li), zcl2016@126.com (C. Zhang).

http://dx.doi.org/10.1016/j.commatsci.2015.11.040
0927-0256/

their excellent mechanical and corrosion properties. Although effects of alloying elements on the impurity elements behavior at Fe GBs, such as Cr on the segregation of multi-H, S, Cl at the bcc Fe GB [17,18], Mn on the P embrittlement of bcc Fe GB [12], have been studied to control the influence of GB segregation, few theoretical research about how alloying elements of the transition series affect impurity elements' behavior at γ-Fe GB system was carried out.

In this paper, by investigating the behaviors of S and B in the γ-FeΣ5 [001] (210) GB with and without alloying elements Cr, Ni, Mn, Co and Mo additions, we explored the role of impurities in GB cohesion and the effects of alloying elements on impurities' behavior at GB to provide a guidance to improve the properties, especially mechanical properties, of AASs GB. As S and B are known to be a GB cohesion embrittler and enhancer respectively in bcc Fe, the comparison offers different insights into the influence of segregants S and B on relative fcc Fe GB cohesion. Based on first-principles calculations, present work systematically describes a fundamental investigation of impurity and alloying elements on γ-Fe GB cohesion.

2. Model and method

We used models of γ-FeΣ5 [001] (210) symmetrical tilt GB and γ-Fe (210) free surface (FS) for the first-principles calculations, as showed in Fig. 1. Clean FS and GB unit cell contain 22 and 40 Fe atoms respectively. Fe sites and GB interstitial sites are indicated by numbers and letters. We refer to the atomic sites as GB0, GB ± 1, GB ± 2, etc. with different colors (red and blue) for Fe or substitutional sites and interstitial sites as a–e, which are presented in both GB and FS cell. For GB systems (Fig. 1(a)), a 21-layer slab was adopted to simulate the clean FeΣ5 (210) GB. The five outermost Fe layer spacings in the GB are fixed in the bulk to reduce free surface effects in the finite thickness slab. There are two GB planes in the GB unit cell, one of which includes GB0 sites and the other includes the GB10 sites, and the alloying elements replaced the Fe (0) sites in the GB core. With 9 layers of Fe atoms in between, the remaining FS–FS and FS–GB interactions were supposed to be sufficiently reduced. For the FS systems, the corresponding clean Fe (210) free surface is simulated by a periodic array of 11 layers of slabs separated by a vacuum layer of 10 Å, which ensure no significant interaction between the slabs, and alloying elements was placed pseudomorphically on the corresponding FS (0) sites. Impurities B and S (introduced artificially in the slab model) were placed at five threefold hollow sites: surface site (a), near surface site (b), interim site (c), near bulk site (d), in bulk site (e), to investigate their segregation behavior in both GB and FS. The (2 × 1) lateral cell of the two slabs was employed to model the calculation system and thus there are two equivalent atomic sites in each layer.

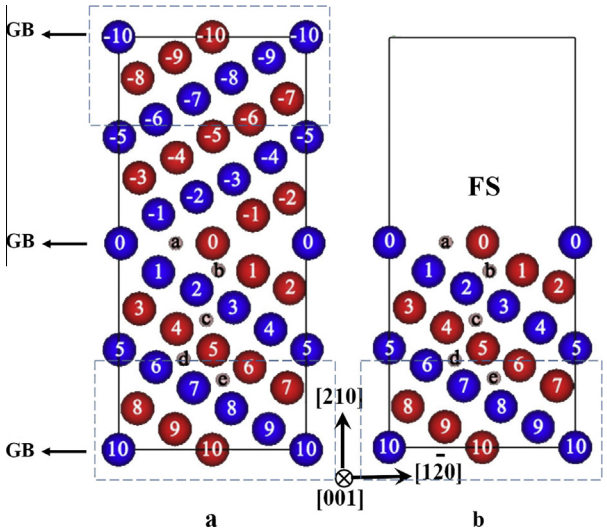

Fig. 1. Model and notation for the structure of Fe (number 0–±10) and impurities (letter a–e) at (a) Fe Σ5 [001] (210) GB and (b) Fe (210) free surface. The blue and red balls represent iron atoms, small pink balls indicate different interstitial sites. Atoms in dashed box are fixed layers. (For interpretation of the references to color in this figure legend, the reader is referred to the web version of this article.)

The CASTEP code (Cambridge Sequential Total Energy Package) [19] based on the density functional theory (DFT) [20,21] was employed to perform our first-principle calculations. We chose the generalized gradient approximation (GGA) in Perdew–Burke–Ernzerhof (PBE) formula [22] when dispose exchange–correlation potential. Ultrasoft pseudopotentials [23] was used for the ion–electron interaction evaluation. A cutoff energy of 300 eV was used for plane-wave expansions. Energy calculations in the Brillouin zone were performed using a [6 × 6 × 1] *k*-point mesh created by the Monkhorst–Pack scheme [24]. To find a more accurate GB model, the atomic positions and all the three vectors lengths (*a*-, *b*- and *c*-axis) are optimized in the whole calculations. The relaxation of atomic positions was carried out, with the thresholds for structures converging: maximum force, energy change, maximum displacement and stress less than 0.05 eV/Å, 2×10^{-5} eV/atom, 2×10^{-3} Å, and 0.1 GPa, respectively. And the final optimized dimensions of the pure GB supercell are $3.45 \times 7.71 \times 15.59$ Å^3.

In order to guarantee the reliability of our calculations, the lattice parameter of bulk fcc Fe was calculated using different functionals (the comparison with Ref. [25] values is listed in Table 1). From the calculation results, we can get that the lattice constant (*a*) and bulk moduli (*B*) value calculated from the GGA-PBE is more consistent with the result given by Ref. [25]. Therefore, GGA-PBE is adopted in the following surface relaxation and energy calculations. Although our calculated lattice parameter value (3.446 Å) is very close to some previously reported values of 3.45 Å [25] and 3.43 Å [26], there is a discrepancy with experimental value of 3.648 Å [27]. These results differences (0.2 Å) are caused by a different calculation method and parameters settings. Given the known paramagnetism of fcc Fe, which cannot be easily modeled within conventional DFT, we chose to model austenite with the nonmagnetic phase of fcc Fe. Thus also leading to the lattice parameter deviation between theory and experiment. Actually, systematic error cancellations are expected because of the same treatment given to the M/Fe GB and corresponding FS systems and all our used energies (binding energy, segregation energy, and strengthening/embrittling energy) are relative values which are obtained by calculating the difference between two absolute energies values. Furthermore, it is well-known that grain boundary energy is about 2/3–1/2 of free surface energy. Grain boundary energies (1.748 J/m^2) for our considered GB are about 2/3–1/2 of the free surface energies (2.873 J/m^2), which is in agreement with the well-known trend. And our calculated free surface energies of clean fcc Fe (210) surface are also close to other theoretical values of 2.83 J/m^2 [28] and 3.62 J/m^2 [29] for fcc Fe (111) surface, validating that our calculation is reliable.

Table 1
Lattice parameters (*a*) and bulk moduli (*B*) of γ-Fe, using different functionals.

Parameter	LDA	GGA-PW91	GGA-PBE	Ref. [26]
a (Å)	3.43	3.435	3.446	3.45
V (Å^3)	38.02	40.54	40.59	41.2
B (GPa)	341.3	307.6	304.8	282

3. Results and discussion

3.1. Behavior of impurities B and S at clean Fe GB

It is necessary to know the behavior of impurities B and S at clean Fe GB, which act as a reference system. In this section, segregation behavior of B and S at optimized GB and their effects on clean GB cohesion are calculated. It is very important for later discussion to determine the stable sites of impurities atoms stayed in clean Fe GB. At first, we discuss which sites in the GB region are occupied by B and S segregation by considering the calculated binding energies of B and S atoms as in Table 2. The binding energy of an impurity atom at GB, E_b, can be calculated as follows [30]:

$$E_b = E_{\text{tot}}^{\text{GB}}\ (\text{nImA}) + nE_{\text{tot}}^{\text{Fe}} - E_{\text{tot}}^{\text{GB}}\ (\text{clean}) - \sum_{i}^{n} E_{\text{tot}}^{\text{ith\_ImA}} \quad (1)$$

where $E_{\text{tot}}^{\text{GB}}$ (ImA) and $E_{\text{tot}}^{\text{GB}}$ (clean) refer to the total energy of the GB unit cell with and without impurities atoms, respectively. $E_{\text{tot}}^{\text{ith\_ImA}}$ is the total energy of every isolated studied impurity atom and $nE_{\text{tot}}^{\text{Fe}}$ is the energy of Fe atoms which are replaced by n substitutional impurities atoms. Thus, a negative E_b value means a stable site for impurity atom and a positive values correspond to an unstable site. When one B or S atom is inserted into the GB vacancy sites (GB *a* to GB *e*), the binding energies show negative values of −5.53 to −9.89 eV. However, when one S atom is substituted for a Fe atom at the other GB sites (GB0 to GB7), the binding energies show positive values of 5.91–6.74 eV. These results mean that B and S prefer the interstitial site to the substitutional one energetically. Thus in subsequent sections, only the interstitial site will be taken into consideration for both B and S.

The binding energy itself cannot decide whether the studied impurity position is the most stable site for their segregation, as it can be evaluated relative to various systems (e.g. with respect to every isolated atom (as done e.g. in Ref. [8]) or with respect to the whole clean GB, as performed here). The tendency of impurities atoms to segregate to or away from a GB/FS should be dictated by its segregation energy (SE), which is defined as the binding energy difference between the GB/FS sites and deep in the bulk material. That is:

$$E_{\text{seg}} = E_b\ (\text{GB}) - E_b\ (\text{bulk}) \quad (2)$$

here E_b (GB) is the binding energy as stated in Section 3.1, and E_b (bulk) is the binding energy when one impurity atom is in the inner bulk environment. According to the definition, the largest negative/positive value corresponds to the most stable/unstable segregation position of the impurity atom. Here, it must be noted that by calculating SE, our objective is to determine the final state or the tendency of elements distribution in GB, not to discuss the diffusion process in great detail. Calculated segregation energies are displayed in Table 3 for impurities in both GB and FS.

As we can see, for both B and S, the segregation energies in GB and FS showed the same tendency for the SE to be negative in all position and SE reaches the largest negative value at GB/FS *a* sites. This obviously suggests that B and S impurities tend to segregate to the GB, which is in agreement with previous experimental and theoretical studies [2,31]. Here it must be noted that initial configurations of GB/FS *b* sites eventually convert into GB *a* sites configuration for both B and S, also indicating that the tendency of GB segregation for B and S. Moreover, the largest negative SE values for B and S are −3.78 and −1.68 eV, respectively, indicating B segregated at GB suppress S segregation at GB distinctly. The presence of these GB segregated impurities elements will considerably modify, generally undesired, the cohesive properties of the GB. The potency of a segregant solute in strengthening or embrittling the GB can be evaluated by the strengthening/embrittling energy, ΔE_{seg}, which should be calculated using follow formula [16]:

$$\Delta E_{\text{seg}} = E_{\text{seg}}^{\text{GB}} - E_{\text{seg}}^{\text{FS}} \quad (3)$$

where $E_{\text{seg}}^{\text{GB}}$ and $E_{\text{seg}}^{\text{FS}}$ are the segregation energy for an impurity atom at the grain boundary (GB) and free surface (FS), respectively. By this calculation method, a solute with a positive ΔE_{seg} value is a more potent embrittler, or vice versa. The estimated value of the GB ΔE_{seg} when either a B or S atom is present at the GB is given in Table 3. The value of ΔE_{seg} for B and S at their segregated positions are negative (−0.91 eV) and positive (1.81 eV) respectively, which clearly indicates that B atom serves as an enhancer but S as an embrittler in the clean Fe grain boundary. Our calculation results are consistent with the experiment.

Table 2
Calculated binding energies (in eV) of impurities B and S (both interstitial and substitutional) in clean Fe GB.

Sites	B	Inter S	Sites	Sub S
GB *a*	−9.89	−7.18	GB0	5.91
GB *b*	−9.24	−7.21	GB1	4.57
GB *c*	−8.16	−5.98	GB3	4.67
GB *d*	−7.40	−6.25	GB5	6.47
GB *e*	−6.11	−5.53	GB7	6.74

Table 3
Calculated segregation energies (in eV) of B and S in the clean γ-Fe FS and GB and the difference in segregation energies.

Sites	B			S		
	$E_{\text{seg}}^{\text{GB}}$	$E_{\text{seg}}^{\text{FS}}$	ΔE_{seg}	$E_{\text{seg}}^{\text{GB}}$	$E_{\text{seg}}^{\text{FS}}$	ΔE_{seg}
a	−3.78	−2.87	−0.91	−1.65	−3.46	1.81
b	−3.13	−2.85	−0.27	−1.68	−3.46	1.78
c	−2.06	−1.42	−0.64	−0.45	−0.13	−0.31
d	−1.29	−0.91	−0.39	−0.72	−0.17	−0.55
e	0	0	–	0	0	–

3.2. Behavior of impurities B and S at alloyed GB

3.2.1. Alloying elements' behavior at GB

We first study the segregation behavior of alloying atoms (Cr, Ni, Mn, Co, Mo) at clean Fe GB and their effects on the GB cohesion. To identify the most energetically favorable segregation site, we swap alloying atoms with Fe atoms at GB I (i = 0, 1, 3, 5, 7) positions to study their segregation behavior. Here, we calculate their segregation energies (SEs) using Eq. (3) to identify at which sites they prefer to stay and site GB7 is chosen as the bulk-like site when calculating E_b (bulk). Our obtained results are displayed in Fig. 2.

As revealed by the calculated SE, all five alloying elements here can steadily stay at the core site in the mirror plane (site GB0) of the GB for the negative SE at GB0. Besides, Ni, Co and Mo prefer to occupy the GB0 site, while Cr and Mn tend to locate at the site in the first layer near GB (site GB1). To recognize and compare their effects on B/S-doped GB cohesive properties, we first look at their role in GB. The strengthening/embrittling energies (ΔE_{seg}) were calculated using Eq. (3) to determine their effects on the clean Fe GB cohesion. As demonstrated in Table 4, there are two categories of alloying atoms. The first one, including Cr, Mn, and Mo, act as the GB enhancer for the calculated ΔE_{seg} are negative at their preferred sites. The second including the rest atoms (Ni and Co) play the GB embrittler role due to the calculated ΔE_{seg} are all positive. Lee et al. also got the same conclusion [15]. Considering the radius of these alloying atoms follow the order: Mo > Cr > Mn > Fe > Co > Ni, we may find that for the substitutional alloying atoms in clean Fe

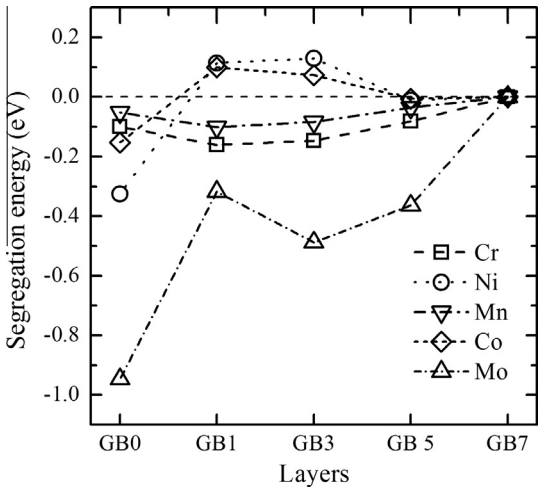

Fig. 2. Calculated segregation energies for alloying atoms at different GB sites.

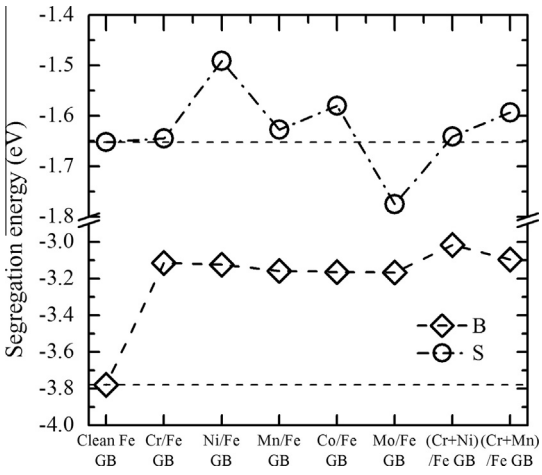

Fig. 3. Calculated segregation energies for B and S at different alloyed GB.

Table 4
Calculated strengthening/embrittling energies (ΔE_{seg}) for alloying atoms at different GB sites.

ΔE_{seg} (eV)	Cr	Ni	Mn	Co	Mo
GB0	0.133	0.703	0.118	0.308	−0.221
GB1	−0.285	0.769	−0.144	0.392	0.236
GB3	−0.182	0.166	−0.133	0.058	−0.427
GB5	−0.228	0.197	−0.172	0.074	−0.364
GB7	0	0	0	0	0

GB, those elements with larger size than Fe serve as cohesive enhancers while elements with smaller radius than Fe play an embrittler role. However, their strengthening/embrittling potencies do not strictly follow this order. Of course, the GB segregation enrichment ratio of alloying atoms should be taken into consideration when discussing their overall effects on GB cohesion.

3.2.2. Alloying effects on the behavior of B and S at GB

In this section, we focus our attention on how alloying atoms affect the behavior of interstitial impurities, thus controlling the impurities-induced embrittlement of the Fe GB. Here, we must note that, although the obtained segregation energies of B and S are lower than those of the alloying elements from our calculations, both of them are negative, meaning that alloying atoms have a tendency (although the tendency of B and S are more obvious) to segregate at GB. Besides, from the point of structure, as the interstitial impurities, B and S are more likely to be affected by the substitutional alloying atoms, not the other way around. In this paper, our focus is mainly alloying effects on the behavior of B and S at the GB. So here our objective is only to demonstrate the effect of alloying atoms additions on the segregation behavior of B and S. Considering GB0 site is stable for all alloying atoms and toward comparison between their effects on B and S behavior, all alloying atoms are substituted Fe (0) atoms. As discussed in Section 3.1, we investigate this issue from their effects on segregation behavior and the strengthening/embrittling behavior of impurities B and S in GB. Calculated segregation energies of B and S in different alloyed GB are shown in Fig. 3. As we can see, the presence of all the alloying elements considered can inhibit B GB segregation to some extent due to the higher segregation energies and has slight effect on S GB segregation except for Ni and Mo, which can inhibit and improve S GB segregation respectively. The strengthening energy of B and the embrittling energy of S in these alloyed GB are estimated and showed in Fig. 4. All of these alloying atoms can impair the enhancement effect of B on GB cohesion due to

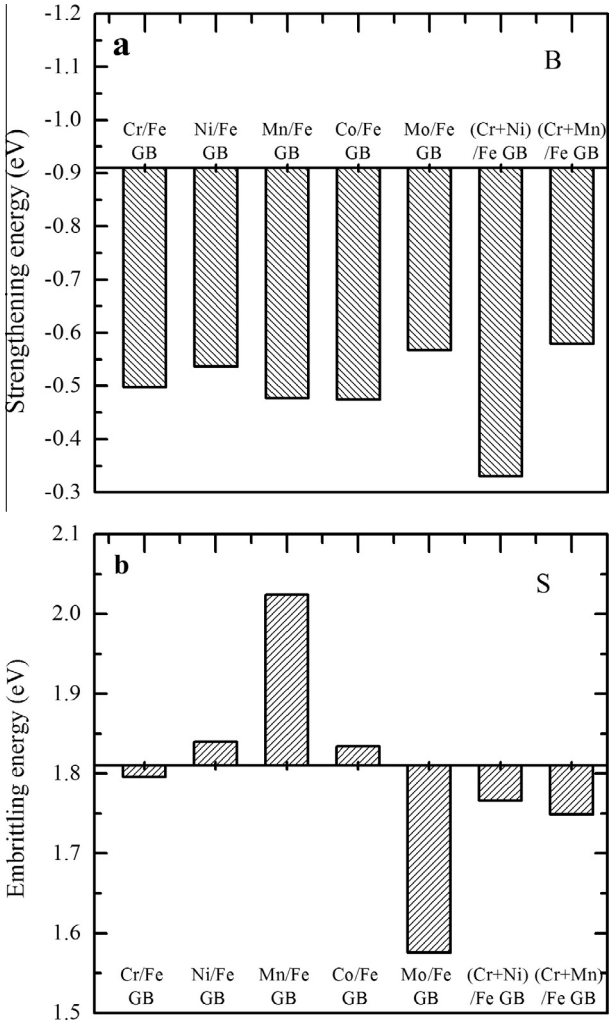

Fig. 4. Calculated strengthening/embrittling energies for B and S at different alloyed GB.

the lower value of $-\Delta E_{seg}$. However, they almost have no impact on the GB embrittlement effect of S, except for Mn and Mo, which strongly enhance and reduce S-induced GB embrittlement respectively. Mn's facilitates embrittlement in the grain boundary is also found by Zhong [12] in P doped Fe GB.

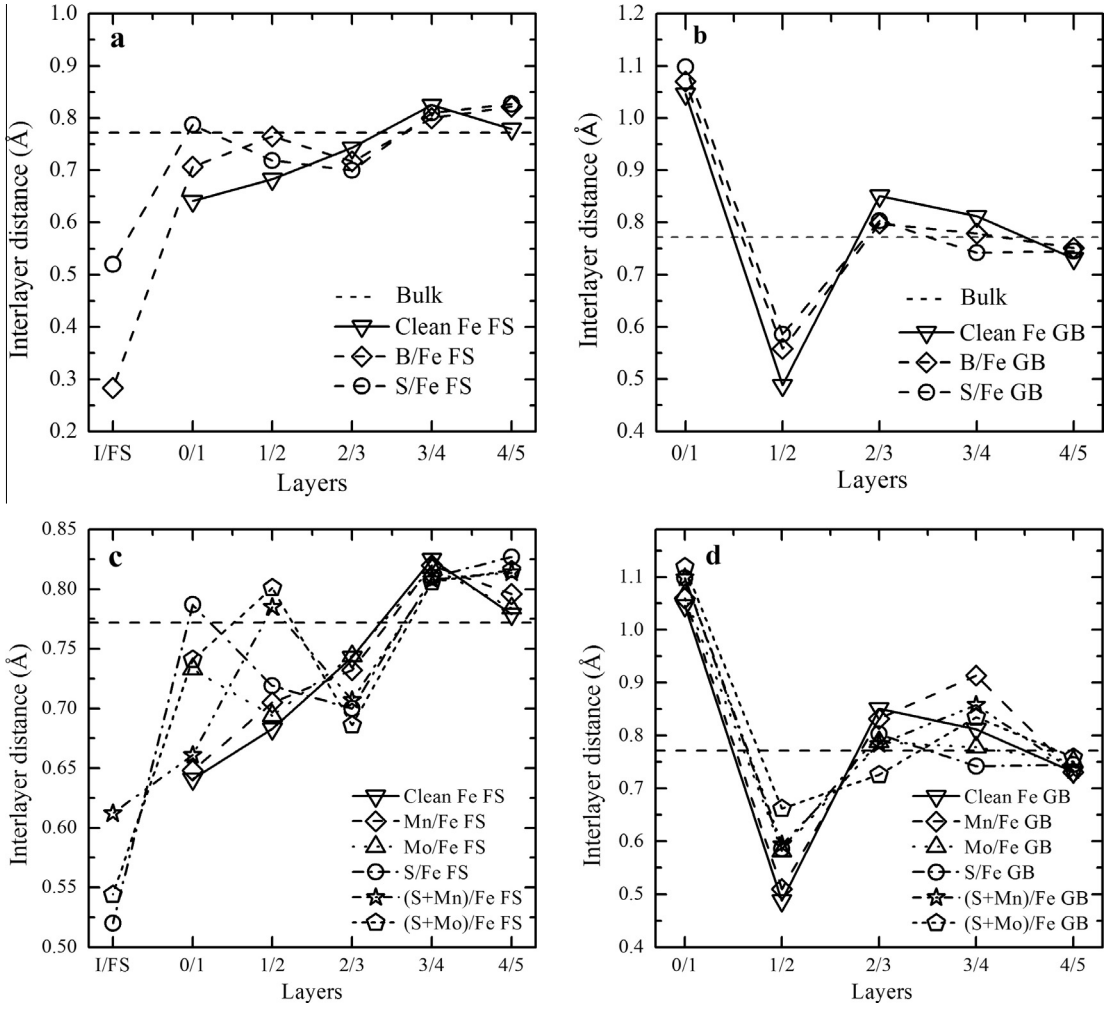

Fig. 5. Calculated interlayer distance in (a) FS, (b) GB systems doped by B and S, (c) S/Fe FS and (d) S/Fe GB systems with alloying atoms addition.

In addition, we investigated the synergistic effect of (Cr + Ni) and (Cr + Mn) on the behavior of B and S in GB. From the calculated embrittling energies of S in alloyed GB (shown in Fig. 4(b)), the remedial effects of their synergy, especially (Cr + Mn), on the GB embrittlement induced by S can be observed. For the direct effect of Mn or Ni, especially for Mn, GB embrittlement S-induced can be strongly enhanced. Associated with Cr together, however, they can reduce S-induced GB embrittlement in Fe–Cr–Ni (Mn) alloys. This result also agrees with the fact that ASSs (a Fe–Cr–Ni alloy) possess excellent mechanic property and the feasibility and advantage of Mn (and N) partially or completely substituting for Ni in ASSs. Based on the above discuss, we can safely conclude that the alloying elements studied can weaken the strengthening effect of B on GB cohesion, and Cr, Mo, (Cr + Ni) and (Cr + Mn) have a remedial effects on S-induced GB embrittlement.

3.3. Atomic structure and total valence charge density

Toward understanding of the original physical and electronic features which governor the segregation behavior and strengthening–embrittling behavior of the alloying and impurities atoms at Fe GB, we carefully compared the interlayer distance and analyzed the total valence charge density of the studied GB and the corresponding FS systems. We first examine the atomic structure. In view of Mn and Mo obvious effects on the cohesive properties of S-induced embrittlement GB, we focus our attention on these correlatable GB systems. The change of interlayer distances is showed in Fig. 5 as a function of the GB sites. In comparison to the pure Fe GB (Fig. 5(b)), although the introduction of both B and S in GB has only a trivial effect (5%) on the structure of GB, the S-induced changes for d_{01} and d_{12} are larger than that of B. In the FS case (Fig. 5(a)), as the adatom on Fe (2 1 0) surface, S tend to more far away from the surface than B ($d_{t\text{-}FS}$) and makes d_{01} change drastic (even larger than the interlayer distance in bulk). All these suggest that S embrittlement effects on GB. Along with the Mn and Mo substitution at GB0 sites in S-doped GB/FS, notable differences in structures occur between the S/Fe and (S + Mn (Mo))/Fe systems. As showed in Fig. 5(d), Mo-induced changes in GB structure can be found from the interlayer distance d_{12}, which rises and by 0.18 Å, and d_{23}, which contracts by 0.13 Å and below the interlayer distance in bulk, indicating the integrated effect of Mo is to liberate the distortion induced by S and to adjust relaxation. In the FS case (Fig. 5(c)), a strong effect of Mn is also seen for $d_{t\text{-}FS}$ (increase by 0.1 Å) and d_{12} (increase by 0.1 Å), demonstrating Mn makes S far away from surface and weakens the interaction between interlayers. As a result, compared with the Fe (0)–Fe (5) bond length in the S/Fe system (3.84 Å for FS and 3.97 Å for GB), the Mn–Fe (5) bond length in (S + Mn)/Fe system is expanded by 0.24 Å and 0.11 Å for the FS and GB, respectively.

The structural changes are in tight connection with the variation in electronic properties. Thus it is necessary to investigate the electronic structure for understanding the atomic interaction.

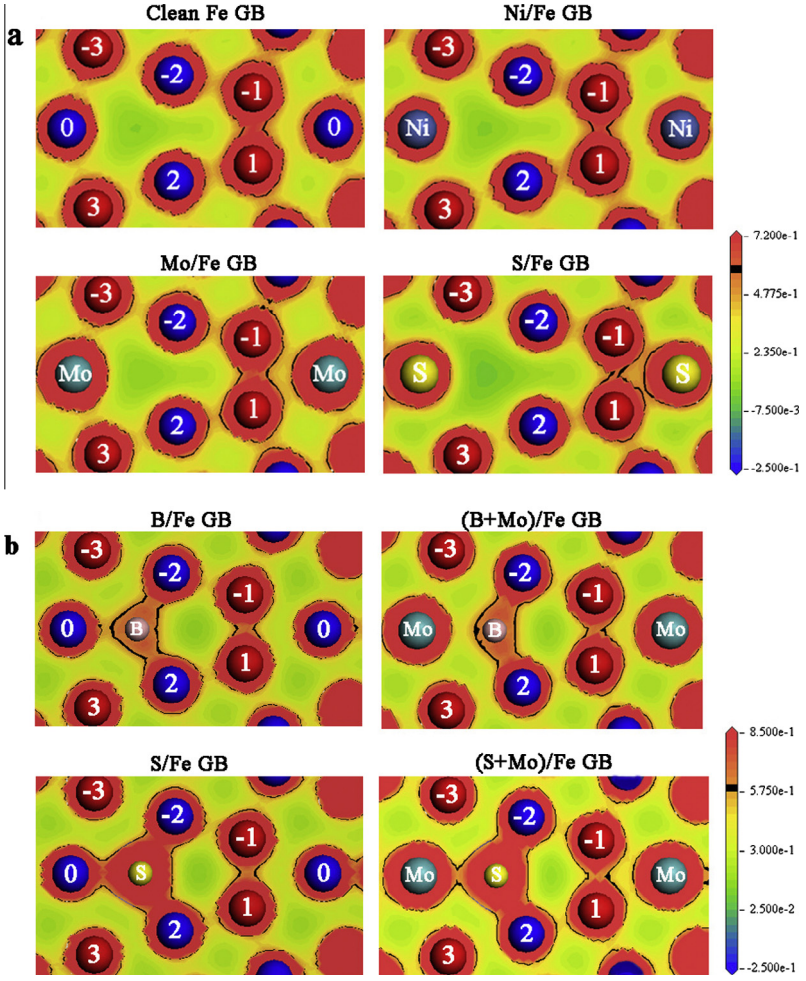

Fig. 6. The calculated total valence charge density for GB with (a) typical alloying atoms substitution and (b) interstitial impurities and Mo addition.

Illuminating figures derived from comparing of the impurity-induced charge redistributions in the different doped GB and the total valence charge density of the corresponding GB is illustrated in Fig. 6. For substitutional alloying atoms (Fig. 6(a)), from the extent of charge accumulations between atoms, their effects on GB cohesion can be attributed to the direct effect arising from the attractive Fe (±3)–M (M = Ni, Mo, substitutional S) and Fe (1)–Fe (−1) interaction, which get strong with enhancer case (Mo), and become weak with embrittler cases (Ni and S) when compared with the clean GB. For interstitial impurities atoms (Fig. 6(b)), the atomic interaction is different. In S/Fe GB, charge depositions can be seen between both S–Fe (0) and S–Fe (±2), suggesting S-induced chemical interaction at GB are divided by lateral and vertical bonding. Embrittlement behaviors of S can be understood from the irretrievable GB expansion by the "embedding" character of the S–Fe bonding, which the vertical bonding (S–Fe (±2)) are not strong enough. By contrast, charge depositions are only found between B and Fe (±2), suggesting that B-induced chemical interaction at GB is all devoted to the vertical attraction and the B–Fe (±2) interactions are more covalent-like. Therefore, B–Fe bonding displays much stronger spatial anisotropy, that is, sturdier perpendicular B–Fe (±2) bonding and feebler horizontal B–Fe (0) bonding. In addition, GB expansion arouse by B is smaller than S. All these demonstrate that the strengthening effect of B derives from the vertical attraction which is strong enough to surpass the GB expansion. The remedial effect of Mo addition on S-induced GB embrittlement can be attributed to the charge transfer from the in-plane state (S–Mo bonding) to the vertical state (S–Fe (±2) bonding), which boosts the vertical attraction.

4. Conclusions

In conclusion, we explored the strengthening- embrittling effect of B and S on the cohesion of γ-FeΣ5 [001] (210) GB with and without alloying elements Cr, Ni, Mn, Co and Mo additions applying first-principles theory calculations. Impurities B and S, which both tend to segregate to the GB, are found to be a cohesive enhancer and a strong embrittler, respectively. All alloying elements additions considered inhibit GB segregation and reduce strengthening effect of B. By the direct effect of Mn or Ni, especially for Mn, S-induced GB embrittlement can be strongly enhanced, while Mo act as an GB enhancer and can strongly reduce the GB embrittlement induced by S. Associated with Cr together, however, Mn or Ni can reduce S-induced GB embrittlement in Fe–Cr–Ni alloys. The examination of the atomic structure the total valence charge density indicates that the embrittlement effect of S on GB derive from the GB expansion which is induced by S and is irretrievable only by the weak vertical (S–Fe (±2)) bonding. By comparison, the dominant vertical attraction which is strong enough to surpass the GB expansion leads B to be a GB cohesion enhancer. The remedial effect of Mo addition can be attributed to its releasing the multilayer relaxation induced by S and its adjusting charge distribution which are transferred from the lateral (S–Mo) bonding to the vertical (S–Fe (±2)) bonding.

Acknowledgements

This work was financially supported by the National Science Foundation of China (No. 51371123), the Specialized Research Foundation of the Doctoral Program for Institution of Higher Education (No. 20131402110003), the Natural Science Foundation of Shanxi Province (Nos. 2014011002-1, 2012011005-7), the China Scholarship Council (CSC) and Opening Fund of State Key Laboratory of Nonlinear Mechanics.

References

[1] B.W. Krakauer, D.N. Seidman, Acta Mater. 46 (1998) 6145–6161.
[2] M. Hashimoto, Y. Ishida, S. Wakayama, R. Yamamoto, M. Doyama, T. Fujiwara, Acta Metall. 32 (1984) 13–20.
[3] Z.W. Li, X.S. Kong, C.S. Liu, Q.F. Fang, Chin. Phys. B 23 (2014) 106107.
[4] D. Wang, N. Gao, F. Gao, Z.G. Wang, Chin. Phys. Lett. 31 (2014), http://dx.doi.org/10.1088/0256-307x/31/9/096801.
[5] X.L. Song, Z.X. Yuan, J. Jia, L.X. Fan, K. Peng, M. Li, P.H. Li, Front. Adv. Mater. Eng. Technol. Pts 1–3 (430–432) (2012) 724–728.
[6] M. Shiga, Masatake Yamaguchi, Hideo Kaburaki, Science 309 (2005) 393–397.
[7] H.H. Kart, M. Uludogan, T. Cagin, Comput. Mater. Sci. 44 (2009) 1236–1242.
[8] M. Yamaguchi, M. Shiga, H. Kaburaki, Mater. Trans. 47 (2006) 2682–2689.
[9] Ruqian Wu, A.J. Freeman, G.B. Olson, Science 265 (1994) 376–380.
[10] T.O.E. Wachowicz, A. Kiejna, Phys. Rev. B 81 (2010) 094104.
[11] R.W.W.T. Geng, A.J. Freeman, G.B. Olson, Phys. Rev. B 62 (2000) 6208–6214.
[12] Lieping Zhong, R. Wu, A.J. Freeman, G.B. Olson, Phys. Rev. B 55 (1997) 11133–11137.
[13] N.H. Heo, J.W. Nam, Y.U. Heo, S.J. Kim, Acta Mater. 61 (2013) 4022–4034.
[14] C.T. Liu, C.L. White, J.A. Horton, Acta Metall. 33 (1985) 213–229.
[15] D.Y. Lee, E.V. Barrera, J.P. Stark, H.L. Marcus, Metall. Trans. A 15A (1984) 1415.
[16] J.R. Rice, J.-S. Wang, Mater. Sci. Eng., A 107 (1989) 23–40.
[17] B. He, W. Xiao, W. Hao, Z. Tian, J. Nucl. Mater. 441 (2013) 301–305.
[18] C.X. Li, S.H. Dang, L.P. Wang, C.L. Zhang, P.D. Han, Mater. Res. Innov. 18 (2014) 1012–1016.
[19] S.J. Clark, M.D. Segall, C.J. Pickard, P.J. Hasnip, M.I.J. Probert, K. Refson, M.C. Payne, Z. Kristallogr. 220 (2005) 567–570.
[20] W. Kohn, L.J. Sham, Phys. Rev. 140 (1965) A1133–A1138.
[21] P. Hohenberg, W. Kohn, Phys. Rev. 136 (1964) B864–B871.
[22] K.B. John, P. Perdew, Matthias Ernzerhof, Phys. Rev. Lett. 77 (1996) 18.
[23] D. Vanderbilt, Phys. Rev. B 41 (1990) 7892–7895.
[24] H.J. Monkhorst, J.D. Pack, Phys. Rev. B 13 (1976) 5188–5192.
[25] D. Jiang, E. Carter, Phys. Rev. B 67 (2003) 214103.
[26] J. Häglund, A. Fernández Guillermet, G. Grimvall, M. Körling, Phys. Rev. B 48 (1993) 11685–11691.
[27] Z.S. Basinski, W. Hume-Rothery, A.L. Sutton, Proc. R. Soc. Lond. A 229 (1955) 459–467.
[28] S.-J. Lee, Y.-K. Lee, A. Soon, Appl. Surf. Sci. 258 (2012) 9977–9981.
[29] Q. Jiang, H.M. Lu, M. Zhao, J. Phys.: Condens. Matter 16 (2004) 521–530.
[30] M. Yamaguchi, M. Shiga, Hideo Kaburaki, Science (2005) 393–397.
[31] X.L. Song, Z.X. Yuan, J.A. Jia, P.H. Li, D. Wang, L.X. Fan, New Mater. Adv. Mater. Pts 1 and 2 (152–153) (2011) 320–325.